WILEY | Hindawi

Research Article

Extensive Field Validations and Corresponding Numerical Investigations for a Cable Tension Estimation Method Based on Local Vibration Measurements

Chien-Chou Chen (iD), **Wen-Hwa Wu** (iD), **Yi-Pei Ko** (iD), **and Gwolong Lai** (iD)

Department of Civil and Construction Engineering, National Yunlin University of Science and Technology, Yunlin 640, Taiwan

Correspondence should be addressed to Wen-Hwa Wu; wuwh@yuntech.edu.tw

To assess the applicability of the tension estimation method using local vibration measurements in a thorough manner, this research work is devoted to systematically investigate the appropriate covering ranges of measurements for different cables. Four cables of three cable-stayed bridges are deliberately chosen to cover a wide range of the cable slenderness parameter. Numerical analyses with finite element models and field validations with real measurements are conducted for these stay cables to demonstrate that the covering range of local measurements can be undoubtedly reduced with the increase of cable slenderness. For a relatively short cable with the slenderness parameter at the order of 4000, the adoption of 1/3 coverage is sufficient to keep a high-level accuracy with at most 1% of error. Besides, 1/4, 1/6, and 1/7 coverages are found adequate to maintain the same level of accuracy for longer cables with the slenderness parameter at the orders of 30000, 55000, and 80000, respectively. With the solid validations presented in the current study, the covering range of the cable for this simplified method employing local vibration measurements can be confidently reduced to greatly alleviate the expense and hard work of sensor installation near the high end.

1. Introduction

For various types of cable-supported bridges, it is undoubted that the corresponding cable members are the most critical force-transmitting components that would straightforwardly reflect their health conditions. As a result, reliable tension estimation for the stay cables of cable-stayed bridges, suspenders of through-type arch bridges, and external tendons of box girder bridges is of vital importance in the structural health monitoring of these bridges. The vibration-based method has been more popularly applied for the tension estimation in engineering practice because it can be customarily excused from certain problems for different direct measurement devices such as installation difficulty, high expense, and poor durability. Such an indirect method typically starts from the identification of cable frequencies with the ambient vibration measurements collected by conventional contact sensors or more advanced noncontact sensors [1–5]. According to the string theory, the most primitive version of the ambient vibration method determines the cable tension with an analytical formula requiring an identified modal frequency, its vibration length, and the corresponding mass per unit length. The accuracy of this type of methods can be further improved by employing more complicated formulas to consider the effects of flexural rigidity [6, 7], gravity sag [8–10], or more realistic boundary conditions [11–14]. Instead of deriving an explicit formula, quite a few finite element (FE) [15–17] or finite difference (FD) [18–20] approaches have also been proposed to estimate the tension value, flexural rigidity, and other parameters by best matching the identified cable frequencies. The latest development for this type of methodology is concentrating on the application of computer vision [21–23] and the detection of real-time cable tension using advanced techniques [22–24].

Even with the above efforts, the tension estimation accuracy of the ambient vibration method may still be

questionable because special anchorage systems with or without rubber constraints are usually installed near the boundaries of a stay cable or suspender. Such practical design details make it particularly difficult to decide an appropriate vibration length required in any tension determination formula or be faithfully modelled in the FE or FD algorithms. To overcome the obstacles coming from the complicated boundary conditions of a realistic cable in a more effective way, the authors pioneered and developed an inventive methodology additionally integrating the mode shape values directly identified from multiple synchronized vibration measurements [25–30]. Based on these mode shape values at various sensor locations for each examined mode, the effective vibration length could be pertinently obtained by optimally fitting the sinusoidal component of the corresponding mode shape function. Using the determined vibration lengths together with the identified modal frequencies for a number of chosen modes, conventional linear regression techniques were then suggested to solve the cable tension and flexural rigidity.

The concept of effective vibration length has also been discussed and utilized in a few studies by the other researchers [31–36] to establish varied versions of the mode shape enhanced method since its first introduction in the last decade [25]. Yu et al. [31] derived an explicit formula for obtaining the effective vibration lengths of prestressed members with the frequency amplitudes of the first two modes at two or three measurement locations, but nonnegligible errors in the subsequent tension estimation were still observed in their numerical simulations with simple boundary conditions. More recently, Yu [32] further incorporated the so-called two-frequency approach with the method initiated by the authors for deciding the effective vibration lengths to expedite the tension prediction of straight cables. Syamsi et al. [33] adopted a similar tactic to handle different end restraints with validations by the experimental data provided in the authors' work [30] and applications on a suspender of an arch bridge. By suggesting an equivalent segmental cable model with a length given by the distance between any two zero-amplitude points of its mode shape, Yan et al. [34] proposed a methodology to deal with any complicated boundary constraints. The tension estimation accuracy of this approach was numerically evaluated using a stay cable with end rotational springs to demonstrate a maximum error less than 5%. Such a method was later generalized and verified by conducting a laboratory test with the vision-based target tracking techniques [35]. It was found from various cases in this experiment that the error of tension estimation can be kept under 3%. In the past two years, this methodology was more elaborately advanced by first combining with the digital image correlation technique [36] and further equipping with the phase-based video motion magnification technique [37] to conduct target-free measurements of full-field cable displacements for a convenient identification of required mode shapes. From the experimental data for a laboratory-scale cable and the real measurements on three suspenders of a half-through arch bridge, the maximum errors of tension estimation in both categories were obtained as 4.0% and 5.4%, respectively.

Moreover, the inclusion of mode shapes has also started to be employed in some FE approaches for the determination of cable tension lately [38, 39].

Compared with the other works considering the mode shapes as reviewed in the previous paragraph, the tension estimation technique cultivated by the authors is especially focused on the proper sensor deployment to ensure high-level accuracy and the convincing verification with either experimental tests or practical applications. Such a method was devised with the assumption of symmetric end conditions in the beginning [25, 26] for simplification and reached the recommendation that three synchronized measurements close to the deck end would be sufficient from the applications on two stay cables. The unsymmetrical boundary constraints were subsequently counted with the addition of a shifting parameter in the sinusoidal mode shape function to discover that at least one sensor should be installed near the far end on top of a few sensors concentrated at the close end in this case [27]. Under such an arrangement of measurements, excellent accuracy in estimating the tension of an external tendon was exhibited by less than 0.5% of difference with respect to the corresponding result obtained from a well-calibrated elasto-magnetic (EM) sensor. This unsymmetrical formulation was further investigated by laboratory experiments of a prestressed strand to demonstrate the accuracy level with the error under 1% [28, 29] and applied to three stay cables [27] as well as several suspenders [28]. The analysis for selected measurements from the full-scale test with an experimental cable of 167.85 m was also reported in a recent article [30] to solidly testify that the threshold of 1% error can be held for this vibration-based approach in comparison with the reference tension value directly gained from the load cell.

Although with successful field applications in abundant tension estimation cases of real cable structures, the necessity of installing at least one sensor near the high end for the developed method based on effective vibration lengths would still seriously obstruct its wide practice on stay cables or suspenders. The authors newly made special efforts to liberate such an unfavorable requirement by carrying out the tension estimation merely with local vibration measurements to fit partial mode shapes for deciding the actually needed half-wavelength of each considered mode [30]. Numerical analyses for two stay cables and experimental verification with a prestressed strand have been conducted in this recent work to explore the acceptable covering range of local measurements and the preferred choice of modes. An important conclusion obtained is that the performance of the method based on local vibration measurements highly relates to the slenderness of cable. Following these promising results, the current study is further carried out to complete extensive field validations for this method together with their corresponding numerical investigations. Such evaluations are aimed to provide specific suggestions for suitable covering ranges of local measurements in the practical applications of different cables with a variety of slenderness. In addition to concisely reviewing the methodology based on local vibration measurements for providing basic backgrounds in the second section, the numerical analysis and

field validation for the investigated cables of three cable-stayed bridges will be presented and discussed in the two following sections.

2. Methodology Based on Local Vibration Measurements

The solutions of the cable vibration equation and the tension estimation method based on the effective vibration lengths determined from multiple measurements will be succinctly described in the first subsection of this section. Furthermore, the second subsection will briefly review the recently proposed approach using local vibration measurements to fit partial mode shapes [30], followed by elaborating a few important guidelines learned from the corresponding numerical and experimental investigations [30] in the third subsection.

2.1. Solution of Cable Vibration Equation and Determination of Effective Vibration Length. Without considering the sag effect, the axial inertial force, and the nonlinear cable motion, the transverse displacement $v(x, t)$ of a cable subjected to an axial tension T is a function of the axial coordinate x and time t. Under free vibration, its equation of motion can be written as

$$\text{EI} \frac{\partial^4 v}{\partial x^4} - T \frac{\partial^2 v}{\partial x^2} + \overline{m} \frac{\partial^2 v}{\partial t^2} = 0, \tag{1}$$

where E stands for Young's modulus, I denotes the cross-sectional area moment of inertia, and $\overline{m}$ represents the mass per unit length. By normalizing x with respect to the cable length L to define a dimensionless variable $\overline{x} = x/L$ in a range of $0 \leq \overline{x} \leq 1$, equation (1) can be further expressed as

$$\frac{\partial^4 v}{\partial \overline{x}^4} - \varepsilon \frac{\partial^2 v}{\partial \overline{x}^2} + \alpha^2 \frac{\partial^2 v}{\partial t^2} = 0, \tag{2}$$

where

$$\varepsilon \equiv \frac{TL^2}{\text{EI}},$$
$$\alpha \equiv \sqrt{\frac{\overline{m}L^4}{\text{EI}}}. \tag{3}$$

With the technique of separation of variables, equation (2) is typically solved by letting $v(\overline{x}, t) = \varphi(\overline{x})Y(t)$ to get the general solutions [29] of $Y(t) = A_1 \sin \omega t + A_2 \cos \omega t$ and

$$\varphi(\overline{x}) = B_1 \sin \delta \overline{x} + B_2 \sin \delta (1 - \overline{x}) + B_3 \sinh \gamma \overline{x} + B_4 \sinh \gamma (1 - \overline{x}), \tag{4}$$

where

$$\delta = \sqrt{\sqrt{\alpha^2 \omega^2 + \frac{\varepsilon^2}{4}} - \frac{\varepsilon}{2}},$$
$$\gamma = \sqrt{\sqrt{\alpha^2 \omega^2 + \frac{\varepsilon^2}{4}} + \frac{\varepsilon}{2}}. \tag{5}$$

It is noteworthy that ω is actually in correspondence to the natural frequency of the cable in rad/sec and $\alpha \omega$ can be regarded as a dimensionless frequency parameter.

When the boundary conditions at both ends of the cable are specified to provide four simultaneous equations from equation (4), the corresponding frequency equations can then be obtained [29]. However, the frequency equations containing the sinusoidal functions of δ and the hyperbolic functions of γ would be too complicated to be analytically solved. The only exception is the case with hinged boundary constraints at both ends, which leads to the following frequency equations:

$$\sin \delta_i = 0 \text{ or } \delta_i = i\pi, \quad i = 1, 2, 3, \cdots, \tag{6}$$

and their associated mode shape functions:

$$\varphi_i(\overline{x}) = \sin \delta_i \overline{x}, \quad i = 1, 2, 3, \cdots. \tag{7}$$

With the definitions of δ, ε, and α in equations (3) and (5), it is easy to analytically express the modal frequencies of cable from the explicit formula of equation (6) as

$$\left(\frac{f_i}{i}\right)^2 = \left(\frac{\omega_i}{2i\pi}\right)^2 = \frac{T + \left(i^2 \pi^2 \text{EI}/L^2\right)}{4\overline{m}L^2}, \quad i = 1, 2, 3, \cdots, \tag{8}$$

in which $f_i = \omega_i/2\pi$ symbolizes the natural frequency of the i-th mode in Hz. In fact, equation (8) can be directly adopted to determine the cable tension with the given mass per unit length $\overline{m}$, vibration length L, and flexural rigidity EI.

Even though an explicit formula like equation (8) is unachievable for more complicated end conditions, equation (4) evidently indicates that the corresponding mode shape functions in these cases would unexceptionally consist of a sinusoidal component $\varphi_i^{(s)}(\overline{x})$ just containing δ and the other hyperbolic component $\varphi_i^{(h)}(\overline{x})$ only involving γ for the i-th mode. Because the hyperbolic function $\sinh \gamma \overline{x}$ is monotonically increasing and $\sinh \gamma (1 - \overline{x})$ is monotonically decreasing with $\overline{x}$ in equation (4), a noticeable contribution from the hyperbolic component $\varphi_i^{(h)}(\overline{x})$ would certainly lead to a mode shape function with large absolute values at $\overline{x} = 0$ and $\overline{x} = 1$. Therefore, the only possibility for a mode shape function to satisfy the typically well constrained boundary conditions at both ends for practical cables is to have a prevailing sinusoidal component and an insignificant hyperbolic component. In other words, the contribution from the hyperbolic component of a mode shape function can be observable merely in a narrow

range close to the boundary and extraction of the sinusoidal component of mode shape function is accordingly feasible in real applications.

Inspired by the above examination, the authors [25–29] proposed a novel concept to solely focus on the sinusoidal component $\varphi_i^{(s)}(\overline{x})$ for advantageously solving the cable frequencies in analytical forms regardless of the complexity of boundary constraints. A simple frequency equation similar to equation (6) can be recovered by just considering the sinusoidal component of the mode shape function:

$$\sin \delta_i \lambda_i = 0 \text{ or } \delta_i = \frac{i\pi}{\lambda_i}, \quad i = 1, 2, 3, \cdots, \tag{9}$$

where λ_i signifies the dimensionless distance between the two zero-crossing positions closest to both ends for the i-th mode. With equation (9), the modal frequencies of cable can again be explicitly expressed as

$$\left(\frac{f_i}{i}\right)^2 = \frac{T + \left(i^2 \pi^2 \mathrm{EI}/\lambda_i^2 L^2\right)}{4\overline{m}\lambda_i^2 L^2}$$

$$= \frac{T + \left(i^2 \pi^2 \mathrm{EI}/L_i^2\right)}{4\overline{m}L_i^2}, \quad i = 1, 2, 3, \ldots. \tag{10}$$

The only difference between equation (10) to deal with complicated end conditions and equation (8) for hinged boundary constraints is that the effective vibration length $L_i = \lambda_i L$ in equation (10) needs to be determined by fitting the sinusoidal component of the corresponding mode shape with the identified values from multiple vibration measurements.

To optimally fit the identified mode shape values at the n measurement locations $x_1, x_2, \cdots, x_n$ for each desired mode, an appropriate error function has been defined [27] as

$$e_i \equiv \sum_{j=1}^{n} \left\{ a_i \sin\left[\frac{i\pi\left(x_j + d_i\right)}{L_i}\right] - \widehat{\varphi}_{ji} \right\}^2, \quad i = i_1, i_2, \ldots, i_m, \tag{11}$$

where $\widehat{\varphi}_{ji}$ denotes the identified mode shape value of the i-th mode at x_j and $i_1, i_2, \cdots, i_m$ are the mode orders of the m chosen modes. Besides, a_i and d_i in equation (11) represent the amplitude coefficient and shifting parameter of the i-th mode, respectively. It should be noticed that there are three unknowns (a_i, d_i, and L_i) to be decided from the optimization of equation (11). Since this is a relatively simple and easily convergent case [26, 27], the Optimization Toolbox of MATLAB is adopted in the current study to obtain the optimal values starting from reasonable initial guesses. With

the effective vibration length L_i determined, equation (10) would become a linear function of the tension T and the flexural rigidity EI if the modal frequencies are identified and the mass per unit length of the cable is given. Finally, the values for T and EI can be conveniently obtained by solving m simultaneous linear equations if a total of m modes are considered. More specifically, the adoption of $m = 2$ leads to a unique solution for T and EI, while classical linear regression techniques can be applied to attain the optimal solution for T and EI if $m > 2$ is taken. Different choices of considered modes would not meaningfully alter the final tension estimation in numerical simulations [25–30], and the selection of three well-fitted modes has been found to work well in the past practical applications by the authors [26–28, 30].

2.2. Sensor Deployment and the Development with Local Vibration Measurements. Since the determination of the effective vibration length L_i plays the most critical role in the aforementioned mode shape enhanced method, a few key issues regarding the sensor deployment for an accurate fitting of the sinusoidal component have been thoroughly investigated in previous studies [26–29]. First of all, the interference of the hyperbolic components in the identified mode shape values should be avoided as much as possible for an excellent fitting of pure sinusoidal components. It was further discovered that the influence range of the hyperbolic component obviously increases with the decreasing value of the dimensionless parameter ε defined in equation (3) to quantitatively indicate the cable slenderness or the dominance of axial tension over bending moment [29]. Specified guidelines for the sensor deployment in practical applications have also been provided by clarifying that the range of meaningful influence from the hyperbolic component is less than 10% of the total length for short cables with $\varepsilon \geq 1000$ and even less than 1% for long cables with $\varepsilon \geq 50000$ [29]. Additionally, it has been extensively explored to conclude that all measurements cannot concentrate at one end of a cable and at least one sensor needs to be installed near the other end for obtaining a reasonable value of the effective vibration length [27]. A convenient approach for tackling such a requirement of covering a full cable range in sensor deployment has been established in a recent work by the authors [30] and will be succinctly discussed in the following paragraph and the next subsection.

By defining $\overline{L}_i \equiv L_i/i$ to represent the half-wavelength for the sinusoidal component of the mode shape in the i-th mode, equations (10) and (11) can be also written as

$$e_i \equiv \sum_{j=1}^{n} \left\{ a_i \sin\left[\frac{\pi\left(x_j + d_i\right)}{(L_i/i)}\right] - \widehat{\varphi}_{ji} \right\}^2 = \sum_{j=1}^{n} \left\{ a_i \sin\left[\frac{\pi\left(x_j + d_i\right)}{\overline{L}_i}\right] - \widehat{\varphi}_{ji} \right\}^2, \quad i = i_1, i_2, \ldots, i_m, \tag{12}$$

$$T + \frac{\pi^2 \mathrm{EI}}{(L_i/i)^2} = 4\overline{m}f_i^2\left(\frac{L_i}{i}\right)^2 \text{ or } T + \frac{\pi^2 EI}{\overline{L}_i^2} = 4\overline{m}f_i^2\overline{L}_i^2, \quad i = 1, 2, 3, \ldots. \tag{13}$$

It is clearly shown in equations (12) and (13) that the required parameter in the formulation of the mode shape based method is essentially the half-wavelength $\overline{L}_i$ of each selected mode, but not the whole effective vibration length L_i. The above inspection opens the door for the potential of cable tension estimation using local vibration measurements [30]. The success of this convenient approach unquestionably depends on the accurate determination of the half-wavelengths of all the considered modes and the appropriate sensor deployments to satisfy such demands. For settling on a favorable sensor deployment that can effectively fit partial mode shapes with a limited covering range of the cable, numerical exploration and experimental verification have been conducted [30], and the gained knowledge will be extracted in the next subsection.

2.3. Knowledge Learned from Recent Numerical and Experimental Investigations. The numerical analysis in the recent work by the authors [30] targeted the shortest cable R01 and longest cable R33 of Chi-Lu Bridge located at Central Taiwan. The FE models using SAP2000 software were constructed for these two cables with the values of ε at around 2000 and 50000, respectively. For methodically evaluating the accuracy of effective vibration lengths (or half-wavelengths) obtained from different sensor deployments, equation (13) was reformulated in that study as to produce a quadratic equation of L_i^2 under given values of $\overline{m}$, f_i, T, and EI. A unique positive value of L_i^2 for the i-th mode can then be solved to serve as the exact solution of effective vibration length for each mode of the FE model.

$$4\overline{m}f_i^2\left(\frac{L_i}{i}\right)^4 - T\left(\frac{L_i}{i}\right)^2 - \pi^2\text{EI} = 0, \quad i = 1, 2, 3, \ldots. \quad (14)$$

With the above FE models, five sensor deployments including the full coverage and four partial coverages with different ranges (1/2, 1/3, 1/4, and 1/5) were considered for comparison. It was observed that the error for the effective vibration length of each mode generally increases with the decreasing covering range of measurements and the decreasing slenderness of cable (or ε value). As for the choice of modes, it is clear that the first few lower modes for which the range of measurements could not cover the major part of their half-wavelengths have to be excluded. Moreover, stable mode shape fitting cannot be guaranteed if the sensor at the far end gets close to the peak or valley positions of the sinusoidal function, and the corresponding modes should be avoided whenever possible. According to these guidelines, the tension values were further estimated for Cable R33 with different combinations of modes under several sensor deployments. The error percentage is less than 0.1% in the case of 1/2 coverage. As for the cases of 1/3 and 1/4 coverages, the corresponding error percentages can still be kept under 0.5%.

To further explore the lower limit of covering range under possible measurement noises and identification errors, experimental tests with a prestressed 7-wire strand were also conducted in the laboratory for verifying the accuracy of the simplified method with local measurements [30]. The dimensionless parameter ε for the experimental strand is estimated at 3300. Similar to the investigations with the numerical models, five sensor deployments corresponding to different ranges of coverage (full, 1/2, 1/3, 1/4, and 1/5) were selected in the experiment. Since no precise values of cable tension and flexural rigidity are available to calculate the exact solution of effective vibration length from equation (14) as in the numerical analysis, the effective vibration length obtained from the case with full coverage was taken as the reference value in this experimental study.

The experimental results were analyzed to evaluate the acceptable covering range of measurements in practice. First of all, the errors in effective vibration length were also found to basically increase with the decreasing range of coverage. Following the guidelines obtained from the numerical investigation and considering the consistency of vibration lengths for well-fitted modes, the selected modes were decided for the cases with different ranges of partial coverages. The tension values corresponding to these partial coverages were then estimated to compare with those with full coverage to obtain the errors at the level of 0.1%, 0.5%, 3%, and 2% for 1/2 coverage, 1/3 coverage, 1/4 coverage, and 1/5 coverage, respectively. In other words, excellent accuracy of estimated tension was demonstrated for the experimental strand with its slenderness similar to a short stay cable when 1/2 and 1/3 covering ranges were adopted. Besides, the accuracy for 1/4 coverage or 1/5 coverage is also at an acceptable level.

3. Investigated Stay Cables and Their Numerical Analyses

As mentioned in the previous section for the numerical results of Cables R01 ($\varepsilon \approx 2000$) and R33 ($\varepsilon \approx 50000$) of Chi-Lu Bridge, the errors for the effective vibration lengths normally increase with the decreasing covering range of measurements and the decreasing value of ε. This indicates that a higher percentage of covering range may be required for a shorter cable generally with a lower value of ε. This research group was fortunate to gain the opportunities of carrying out the field validation for the method based on local vibration measurements by executing cable tension measurement projects on three cable-stayed bridges recently. To more broadly examine the lower limit of covering range for local vibration measurements in practical applications, the investigated stay cables were purposely selected to cover a wide range of ε. The numerical analyses for these cases are first conducted and discussed in this section to evaluate the

appropriate covering range of local measurements for a variety of stay cables in a systematic way. The results from field measurements to serve as concrete verifications for the method using local vibration measurements will be presented in the next section.

3.1. Cable CR06 of Da-Chih Bridge.

With its photo displayed in Figure 1(a), Da-Chih Bridge is an unsymmetrical single-pylon cable-stayed bridge situated in Taipei City of Taiwan. It comprises a steel pylon with a height of 70 m in the shape of a fishing pole, a main span with a length of 195 m, and a side span with a length of 50 m. Six pairs of stay cables are arranged along the centerline of girder to support the main span, as portrayed in Figure 1(b). Additionally, there are 10 backstay cables divided into two symmetric groups with respect to the pylon on the side of the side span. Ambient vibration measurements were conducted on Cable CR06 with an inclination angle of 79° and are specified by a red solid circle in Figure 1(b). The adopted parameters in the numerical analysis of this cable including the values of cable tension and flexural rigidity taken from the results estimated with real measurements are listed in Table 1. According to these parameters, the corresponding value of ε for Cable CR06 is approximately 4000 and its FE model consisting of 4749 frame elements with a length of 1 cm is constructed using SAP2000 software. The actual anchorage system is simulated by a fixed end and a pair of linear springs located at the two adjacent nodes near the rubber location, as shown in Figure 2, to mimic the elastic constraints from rubber in both the transverse and rotational directions. Furthermore, the spring coefficient of the spring element is assumed to be 8×10^6 N/m such that the simulated cable frequencies can well match those identified from real measurements. More specifically, the discrepancies between the simulated and identified modal frequencies of the first 10 modes are all kept under 0.5% for Cable CR06.

Modal analysis with the above FE model can then be carried out to obtain the simulated modal frequencies and mode shapes that serve as the identified modal parameters. As also plotted in Figure 2, four sensor deployments including the full coverage and three partial coverages with different ranges (1/2, 1/3, and 1/5) are chosen for comparison. Between spring constraints of the FE model, four nodes along this portion are selected as the presumed sensor locations in each deployment. The three sensor locations close to the left end ($x = 0.03L$, $0.05L$, and $0.07L$) are the same for all the four deployments and symbolized by red dots. The spacing for these three sensor locations is consistently taken as $0.02L$ in this study to balance the needs of mode shape fitting and practical installation convenience. The position of the first sensor from left is determined in accordance with the consideration of adequately eliminating the interference from hyperbolic components as mentioned in the previous section. In general, the required distance between the first sensor and the adjacent boundary decreases with the increasing value of the cable slenderness parameter ε, and more details can be found in a previous work [29]. As for the fourth sensor denoted by a blue dot in each deployment, its location is changed in different cases of considered coverage to encompass various ranges (full, 1/2, 1/3, and 1/5). In addition, the concern of hyperbolic components is also taken into account for the case of full coverage.

For each sensor deployment, the mode shape values for each mode are then optimally fitted to obtain the corresponding effective vibration length L_i (or equivalently the half-wavelength $\overline{L}_i$) with equation (12). Considering the second to the twelfth modes that will be used to estimate the tension values in different cases, the optimal effective vibration lengths for these modes with various sensor deployments are determined to compare with the corresponding exact values solved from equation (14) in Table 2. As reviewed in the previous section, the accuracy of the effective vibration lengths for the first few lower modes would severely deteriorate if the range of measurements could not cover the major part of their half-wavelengths. Consequently, the comparison for these modes is not included in Table 2. Also highlighted by bold-face numbers in Table 2, it is evident that the odd modes for 1/2 coverage, the fifth, eighth, and eleventh modes for 1/3 coverage, and the eighth mode for 1/5 coverage are all with relatively more significant errors than those of the other modes. As unveiled in the previous study [30] and also reviewed in the previous section, this phenomenon is caused by the sensor location at the far end. When such a measurement is taken at a position very close to the peaks (or valleys) of the corresponding sinusoidal function, the flat slope of an extremum would make it particularly difficult to obtain robust fitting for an accurate effective vibration length.

Following the guidelines to avoid the lower modes whose half-wavelengths cannot be sufficiently covered by measurements and the modes for which the sensor at the far end is located near the peak/valley positions, the estimated tension values are presented in Table 3 for the simulation of Cable CR06. In the case of 1/2 coverage, the 2nd, 4th, and 6th modes are first selected to obtain a tension value of 4097.2 kN using equation (10). The other choice of the 8th, 10th, and 12th modes yields a tension value of 4099.4 kN. With respect to the input value of 4080 kN as listed in Table 1, the error percentages for these two independent mode selections are both less than 0.5% to convincingly testify the accuracy and stability of the proposed method. Regarding the case of 1/3 coverage, two sets of mode selection both exhibit less than 1% of error in tension estimation. But for the sensor deployment with 1/5 coverage, the corresponding accuracy further declines to possibly reach an error percentage beyond 2%. In other words, it is demonstrated in this numerical example of $\varepsilon \approx 4000$ that an excellent accuracy level with less than 1% of tension estimation error can be ensured with 1/2 and 1/3 coverages, but not with a more limited measurement range of 1/5 coverage.

3.2. Cable F07 of Shih-Chien Bridge.

Shih-Chien Bridge, as shown in Figure 3(a), is an unsymmetrical single-pylon and single-span (100 m) cable-stayed bridge located in Keelung City at the very northern part of Taiwan. Its reinforced
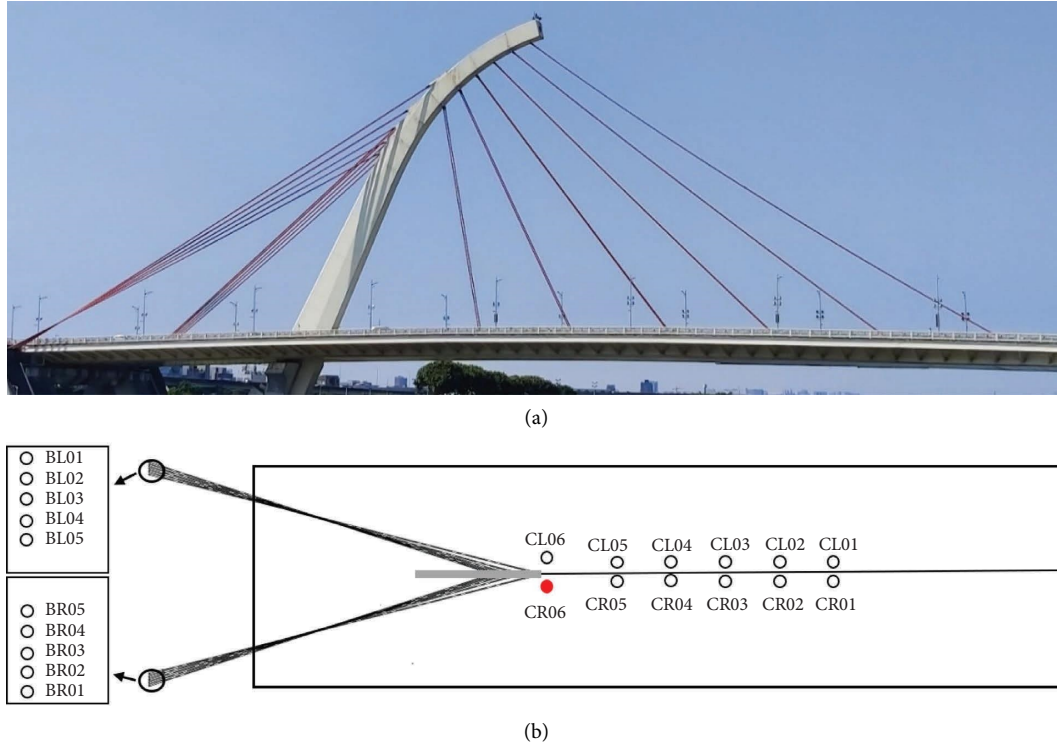
(a)

(b)

Figure 1: Da-Chih Bridge and its cable arrangement. (a) Photo. (b) Cable arrangement.

Table 1: Parameters for the investigated stay cables.

Bridge	Cable no.	Total length (m)	Distance from rubber to anchorage (m)		Mass per unit length $\overline{m}$ (kg/m)	Flexural rigidity EI (10^6N·m²)	Tension T (kN)
			Left	Right			
Da-Chih	CR06	47.49	2.74	2.88	90.58	2.270	4080
Shih-Chien	F07	100.61	2.94	5.88	39.36	0.247	751.6
Kao-Ping-Hsi	SB106	160.41	3.81	5.18	144.3	3.959	8449
	SF100	327.32	5.47	4.17	130.9	6.742	4983

concrete pylon is composed of two columns connected by two horizontal beams, and it stands 62 m tall. As illustrated in Figure 3(b), there are totally 10 pairs of stay cables arranged in the harp shape with the same inclination angle of 26° in this bridge. Ambient vibration measurements were taken on Cable F07 indicated by a red solid circle in Figure 3(b). Similarly, the values of cable tension and flexural rigidity estimated from real measurements are employed to perform the numerical analysis of this cable, and they are also listed in Table 1 together with the other parameters. Based on these parameters, the corresponding value of ε for Cable F07 is roughly 30000 and its FE model constructed with SAP2000 contains 10061 frame elements with a length of 1 cm. As depicted in Figure 4, the actual anchorage system is also simulated by a pair of linear springs with the coefficient of 10^6N/m near the rubber location to closely duplicate the cable frequencies identified from real measurements.

Four sensor deployments incorporating the full coverage and three partial coverages with different ranges (1/3, 1/4, and 1/6), as also displayed in Figure 4, are adopted for the numerical investigation of this cable. The position of the first sensor closest to the left end is assigned at $x = 0.01L$ considering the larger value of ε associated with this cable, and those for the next two sensors are allocated at $x = 0.03L$ and $x = 0.05L$ to keep the same distribution as in the previous subsection. On the other hand, the position of the fourth sensor represented by a blue dot in each deployment is adjusted to cover the intended range. Focusing on the third to the thirteenth modes that will be used to estimate the tension values in various sensor deployments, their optimally fitted effective vibration lengths are obtained from the corresponding mode shape values and compared in Table 4 with the exactly solved values. As also indicated by bold-face numbers in this table, relatively larger errors due to the sensor location at the far end occur in the eighth and
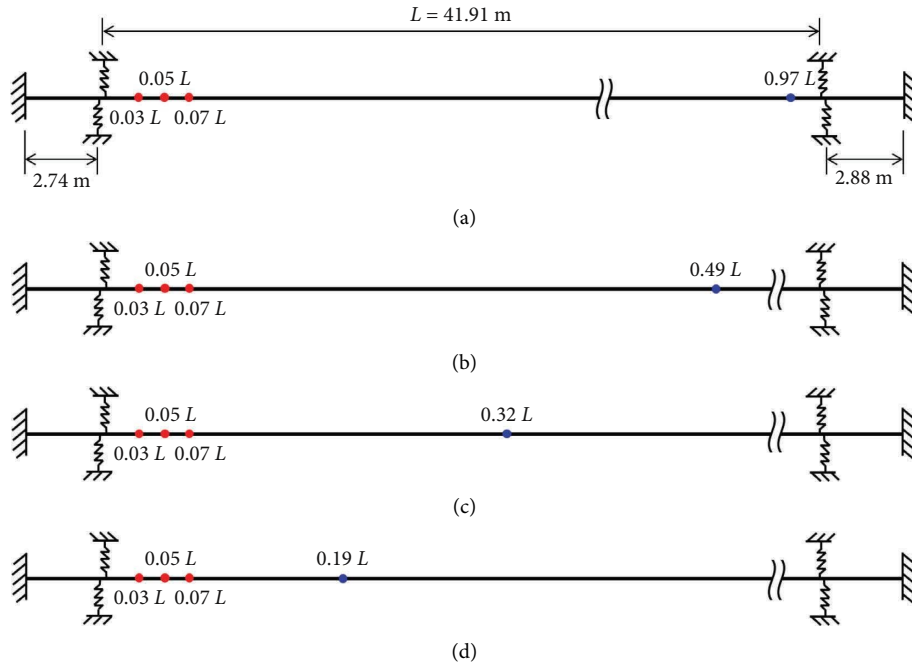
Figure 2: Finite element model and sensor deployments for Cable CR06 of Da-Chih Bridge. (a) Full coverage. (b) 1/2 coverage. (c) 1/3 coverage. (d) 1/5 coverage.

Table 2: Error comparison of effective vibration lengths for Cable CR06 of Da-Chih Bridge.

Covering range of measurements	Error in effective vibration length for each mode (%)										
	2nd mode	3rd mode	4th mode	5th mode	6th mode	7th mode	8th mode	9th mode	10th mode	11th mode	12th mode
Full	0.17	0.20	0.10	0.14	0.10	0.08	0.07	−0.13	0.02	0.03	−0.01
1/2	0.21	**0.74**	0.12	**0.25**	0.11	**0.24**	0.07	**0.27**	−0.01	**0.16**	−0.04
1/3	—	0.20	0.15	**0.37**	0.19	0.24	**−0.29**	0.02	0.12	**−1.37**	−0.08
1/5	—	—	—	0.50	0.42	0.50	**2.67**	−0.16	0.03	0.12	0.37

Table 3: Estimated tension and accuracy for Cable CR06 of Da-Chih Bridge.

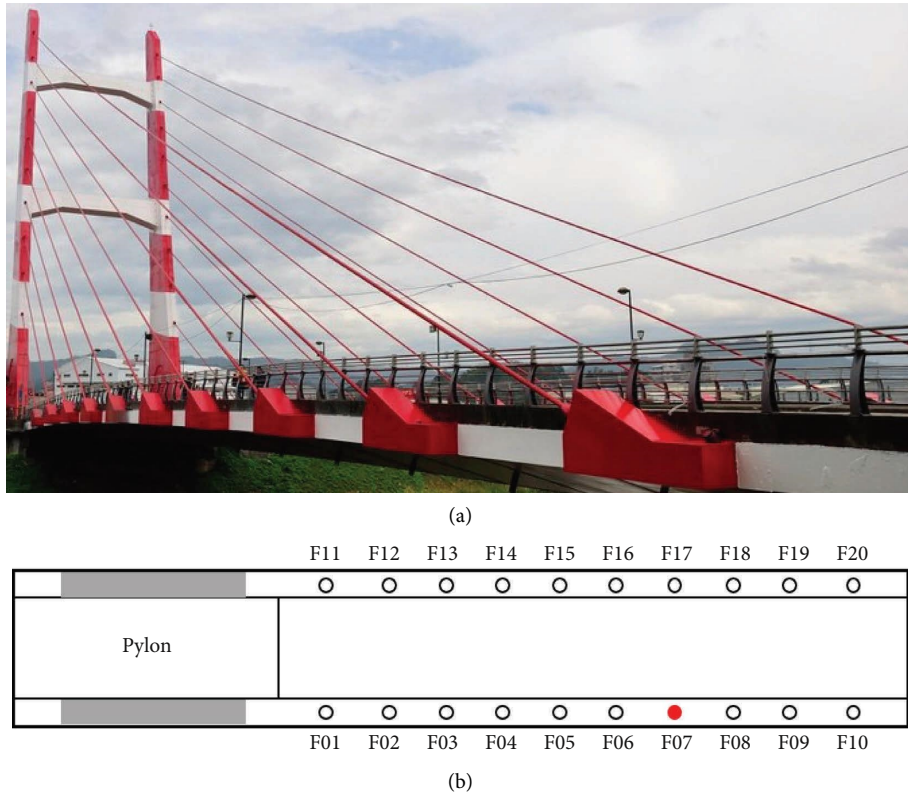| Covering range of measurements	Selected mode	Modal frequency (Hz)	Effective vibration length (m)	Estimated tension (kN)	Percentage of error (%)
1/2	2	5.128	41.741		
	4	10.431	41.758	4097.2	0.42
	6	16.072	41.844		
	8	22.190	41.943		
	10	28.888	42.048	4099.4	0.47
	12	36.219	42.221		
1/3	3	7.747	41.846		
	4	10.431	41.773	4111.2	0.76
	6	16.072	41.878		
	7	19.064	41.952		
	9	25.462	41.986	4114.5	0.84
	10	28.888	42.102		
1/5	5	13.200	41.958		
	6	16.072	41.973	4117.9	0.93
	7	19.064	42.059		
	9	25.462	41.913		
	10	28.888	42.063	3988.5	−2.24
	11	32.475	42.186		

(a)

(b)

FIGURE 3: Shih-Chien Bridge and its cable arrangement. (a) Photo. (b) Cable arrangement.
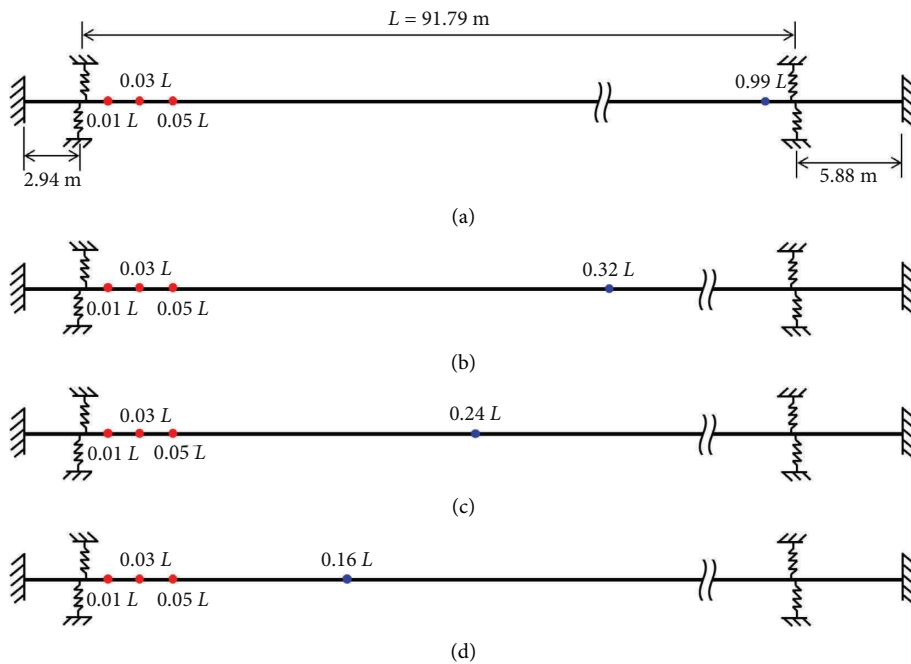

(a)

(b)

(c)

(d)

FIGURE 4: Finite element model and sensor deployments for Cable F07 of Shih-Chien Bridge. (a) Full coverage. (b) 1/3 coverage. (c) 1/4 coverage. (d) 1/6 coverage.

eleventh modes for 1/3 coverage, the sixth and tenth modes for 1/4 coverage, and the ninth and tenth modes for 1/6 coverage.

Abiding by the same guidelines to avoid inappropriate modes, the tension values of Cable F07 are estimated with two independent mode selections for each sensor

TABLE 4: Errors in effective vibration lengths for Cable F07 of Shih-Chien Bridge.

Covering range of measurements	Error in effective vibration length for each mode (%)										
	3rd mode	4th mode	5th mode	6th mode	7th mode	8th mode	9th mode	10th mode	11th mode	12th mode	13th mode
Full	0.01	0.03	0.01	0.02	0.01	0.02	0.00	0.00	0.01	0.00	0.00
1/3	0.03	−0.13	0.01	0.04	−0.02	**0.12**	0.00	−0.02	**1.00**	−0.02	0.03
1/4	—	0.10	0.11	**0.18**	−0.01	0.06	0.02	**0.08**	0.05	−0.01	0.02
1/6	—	—	—	0.10	0.00	0.10	**0.14**	**0.16**	0.09	0.00	0.03

deployment and listed in Table 5. For the case of 1/3 coverage, the selection of the 3rd, 4th, and 5th modes results in a tension value of 752.2 kN, while an alternative choice of the 6th, 7th, and 9th modes produces a tension value of 752.0 kN. Both values are very close to the input tension value of 751.6 kN shown in Table 1 and with less than 0.1% of error percentages. As for the cases of 1/4 coverage and 1/6 coverage, less than 0.5% of error percentages in tension estimation are found with two different mode selections for each sensor deployment. Overall, it is obvious from this numerical example of $\varepsilon \approx 30000$ that the accuracy in tension estimation of the adopted method performs even better than that in the previous subsection for Cable CR06 with $\varepsilon \approx 4000$ to justify further reduction in the covering range of measurements.

3.3. Cables SB106 and SF100 of Kao-Ping-Hsi Bridge.
Sitting between Kaohsiung City and Pingtung County in Southern Taiwan, Kao-Ping-Hsi Bridge is an unsymmetrical single-pylon cable-stayed bridge consisting of a main span made by steel box girders and a side span built with prestressed concrete box girders. As pictured in Figure 5(a), its reinforced concrete pylon is 183.5 m tall, its main span is 330 m in length, and its side span is 180 m in length. On each side of the pylon, 15 pairs of stay cables are spread along the centerline of girder in the semifan shape. Figure 5(b) illustrates the distribution of the 30 cables on the north (upstream) side and the other 30 cables on the south (downstream) side. As marked by the two red solid circles in Figure 5(b), Cable SB106 with an inclination angle of 39° and Cable SF100 with an inclination angle of 23° were picked to perform ambient vibration measurements. Using the input parameters listed in Table 1, the corresponding value of ε for Cable SB106 is close to 55000 and its SAP2000 model is established with 16041 frame elements of 1 cm length. Moreover, the ε value of Cable SF100 is almost 80000 and its FE model comprises 16366 frame elements with a length of 2 cm. As portrayed in Figures 6 and 7, a pair of linear springs with the coefficients 2×10^6 N/m for Cable SB106 and 4×10^6 N/m for Cable SF100 is also added near the rubber location to simulate the actual anchorage system and intimately reproduce the identified cable frequencies.

As drawn in Figures 6 and 7, four sensor deployments including the full coverage and three partial coverages (1/3, 1/6, and 1/8 for Cable SB106 and 1/4, 1/7, and 1/10 for Cable SF100) are assumed for the numerical analyses in this subsection. Again, the three sensor locations close to the left end ($x = 0.01L$, $0.03L$, and $0.05L$) are the same for all the four deployments and signified by red dots. Regarding the fourth sensor location, it is also changed in each deployment to enclose the aimed range. For Cable SB106, its optimal effective vibration lengths for the third, fourth, and sixth to 15th modes decided from fitting the corresponding mode shape values are compared with the exactly solved values in Table 6. Similar results for the fourth, fifth, seventh to 15th, 17th, and 18th modes are also arranged in Table 7 for Cable SF100. In these two tables, the presented modes are considered by the employment to estimate the tension values in various cases and the bold-face numbers are also used to indicate the more considerable errors coming from the sensor location at the far end.

In Table 8, the tension values of Cable SB106 are estimated with two different mode selections for each sensor deployment. For the case of 1/3 coverage, both estimated tension values (8435.4 kN and 8446.0 kN) are with less than 0.2% of error percentages compared to the input tension value of 8449 kN. Regarding the cases of 1/6 coverage and 1/8 coverage, it is discovered that two independent mode selections for each sensor deployment consistently yield less than 0.5% of error percentages in tension estimation. Similar comparison of estimated tension values for Cable SF100 is exhibited in Table 9. For the case of 1/4 coverage, the error percentages of the two estimated tension values (4975.4 kN and 4986.0 kN) are both less than 0.2% with respect to the input tension value of 4983 kN. As for the cases of 1/7 coverage and 1/10 coverage, less than 0.5% of error percentage in tension estimation is steadily observed in different mode selections.
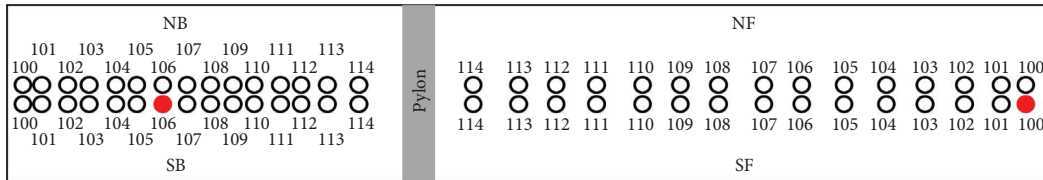
Comprehensively comparing the numerical results listed in Tables 3, 5, 8, and 9 for the four examined stay cables, it is apparently demonstrated that the covering range of sensor deployment in the methodology based on local vibration measurements can be reduced with the increasing ε value of the cable. More specifically, 1/3 coverage for Cable CR06 of Da-Chih Bridge ($\varepsilon \approx 4000$), 1/6 coverage for Cable F07 of Shih-Chien Bridge ($\varepsilon \approx 30000$), 1/8 coverage for Cable SB106 of Kao-Ping-Hsi Bridge ($\varepsilon \approx 55000$), and 1/10 coverage for Cable SF100 of Kao-Ping-Hsi Bridge ($\varepsilon \approx 80000$) are adequate to keep the error percentage in tension estimation under 1%. In other words, this method can be brought into full play for longer cables which would gain more benefits from lowering the sensor installation height.

TABLE 5: Estimated tension and accuracy for Cable F07 of Shih-Chien Bridge.

Covering range of measurements	Selected mode	Modal frequency (Hz)	Effective vibration length (m)	Estimated tension (kN)	Percentage of error (%)
1/3	3	2.257	92.017		
	4	3.013	92.036	752.2	0.10
	5	3.772	92.020		
	6	4.536	92.039		
	7	5.304	92.040	752.0	0.08
	9	6.859	92.051		
1/4	4	3.013	92.098		
	5	3.772	92.115	754.2	0.36
	7	5.304	92.023		
	8	6.078	92.101		
	9	6.859	92.068	752.1	0.08
	11	8.442	92.132		
1/6	6	4.536	92.115		
	7	5.304	92.035	750.3	−0.15
	8	6.078	92.224		
	11	8.442	92.163		
	12	9.246	92.099	754.6	0.42
	13	10.060	92.148		

(a)

(b)

FIGURE 5: Kao-Ping-Hsi Bridge and its cable arrangement. (a) Photo. (b) Cable arrangement.

4. Field Validation

Even with outstanding numerical results as presented in the previous section, the performance of the proposed method may be deteriorated in realistic applications due to potential measurement noises and identification errors. The analyses of real measurements lately taken from the four investigated stay cables will be probed in this section to more persuasively endorse the practical effectiveness of the method using local vibration measurements.

4.1. Cable CR06 of Da-Chih Bridge. With a duration of 300 sec and a sampling rate of 200 Hz, the high-accuracy MEMS capacitive accelerometers (SDI2210-002) produced by Silicon Designs were utilized to record the in-plane vibration component for Cable CR06 of Da-Chih Bridge. As shown in Figure 8 with an illustration and an on-site photo, the sensor deployment was designed to simultaneously implement the full coverage and two partial coverages (1/2 and 1/3). The three accelerometers close to the deck end were located at $x = 0.03L$, $0.05L$, and $0.07L$ in accordance with the
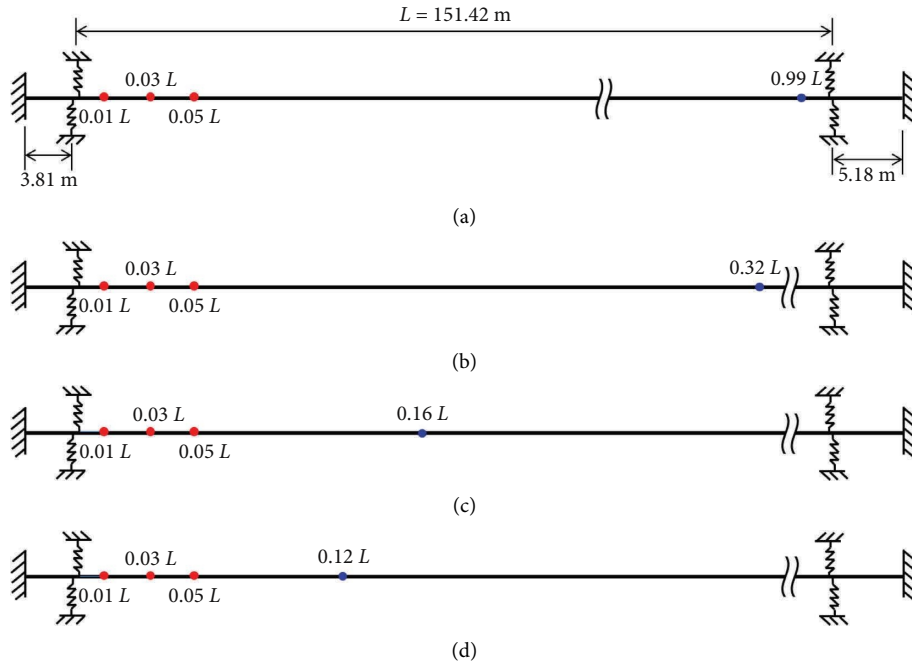
Figure 6: Finite element model and sensor deployments for Cable SB106 of Kao-Ping-Hsi Bridge. (a) Full coverage. (b) 1/3 coverage. (c) 1/6 coverage. (d) 1/8 coverage.
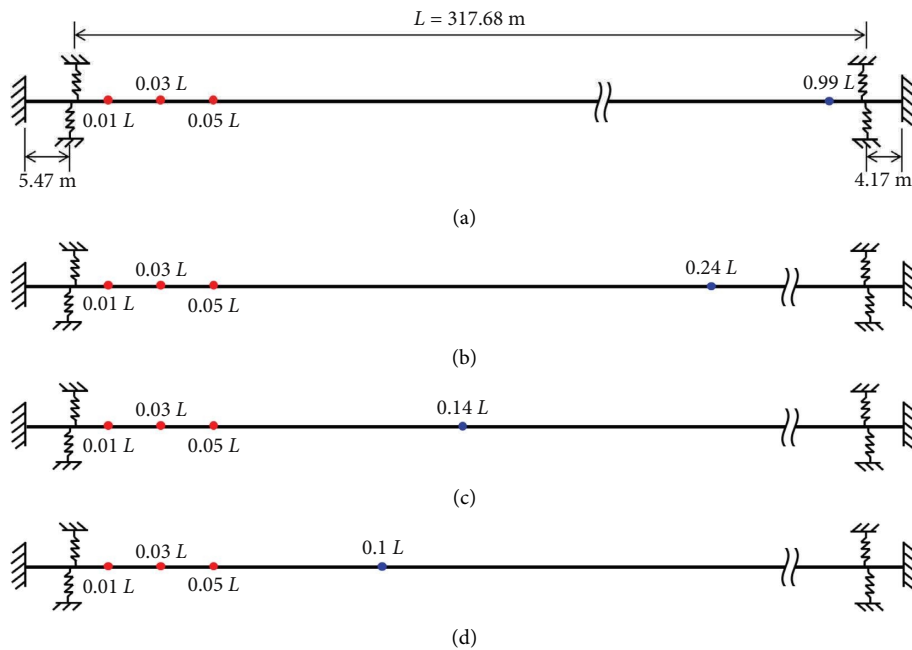

Figure 7: Finite element model and sensor deployments for Cable SF100 of Kao-Ping-Hsi Bridge. (a) Full coverage. (b) 1/4 coverage. (c) 1/7 coverage. (d) 1/10 coverage.

lower value of $\varepsilon \approx 4000$ in this case. The fourth accelerometer at the far end was installed at $x = 0.49L$ for 1/2 coverage and at $x = 0.32L$ for 1/3 coverage, respectively. It should be particularly noted that two accelerometers were employed near the pylon end at $x = 0.86L$ and $0.88L$ for the full coverage. Because of the height limit of 40 m for the hired mobile crane, $x = 0.88L$ is the farthest position at the cable that can be reached and the other sensor at $x = 0.86L$ is added to compensate the possibly lost fitting accuracy at the pylon end.

TABLE 6: Errors in effective vibration lengths for Cable SB106 of Kao-Ping-Hsi Bridge.

Covering range of measurements	Error in effective vibration length for each mode (%)											
	3rd mode	4th mode	6th mode	7th mode	8th mode	9th mode	10th mode	11th mode	12th mode	13th mode	14th mode	15th mode
Full	0.04	0.04	0.05	0.04	0.04	0.04	0.04	0.04	0.04	0.03	0.04	0.03
1/3	0.05	−0.12	0.07	0.01	**0.14**	0.04	0.03	**0.10**	0.02	0.04	**0.60**	0.00
1/6	—	—	0.13	0.08	0.03	**0.42**	0.11	0.10	0.08	0.08	0.15	**0.43**
1/8	—	—	—	—	0.16	0.13	0.13	**0.20**	**0.65**	0.12	0.08	0.09

TABLE 7: Errors in effective vibration lengths for Cable SF100 of Kao-Ping-Hsi Bridge.

Covering range	Error in effective vibration length for each mode (%)											
	4th mode	5th mode	7th mode	8th mode	9th mode	10th mode	11th mode	12th mode	13th mode	14th mode	15th mode	17th mode	18th mode
Full	0.01	0.01	0.01	0.01	0.01	0.01	0.01	0.01	0.01	0.00	0.00	0.00	0.00
1/4	0.03	−0.03	0.07	0.04	0.03	−0.02	0.04	0.04	0.02	0.07	0.01	0.03	0.05
1/7	—	—	0.07	0.07	0.05	0.05	**0.31**	**0.12**	0.08	0.07	0.06	**0.17**	**0.24**
1/10	—	—	—	—	—	0.11	0.14	0.13	0.15	**0.20**	**0.28**	0.15	0.06

TABLE 8: Estimated tension and accuracy for Cable SB106 of Kao-Ping-Hsi Bridge.

Covering range of measurements	Selected mode	Modal frequency (Hz)	Effective vibration length (m)	Estimated tension (kN)	Percentage of error (%)
1/3	3	2.361	153.917		
	4	3.150	153.673	8435.4	−0.16
	6	4.734	153.999		
	7	5.528	153.941		
	9	7.127	154.048	8446.0	0.03
	10	7.931	154.072		
1/6	6	4.734	154.098		
	7	5.528	154.049	8468.5	0.23
	10	7.931	154.204		
	11	8.739	154.228		
	12	9.550	154.254	8476.5	0.33
	13	10.366	154.318		
1/8	8	6.326	154.199		
	9	7.127	154.192	8484.0	0.41
	10	7.931	154.229		
	13	10.366	154.377		
	14	11.187	154.384	8478.0	0.34
	15	12.012	154.488		

From the measurements on Cable CR06 and the corresponding Fourier spectra, the modal frequencies and mode shape values for the first eight modes can be confidently identified. In particular, the mode shape values at the measured points for a specific mode can be accurately estimated by normalizing the complex-valued Fourier transforms of measurements at the corresponding modal frequency with respect to the one with the largest amplitude [26, 27]. Since the mode shape values are theoretically real, the real parts of the estimated values from the above procedures are taken as the mode shape values and their trivial imaginary parts can be used to indicate the effectiveness of these measurements. For the first eight modes of Cable CR06, all the imaginary parts of such estimated values are less than 10% of their corresponding real parts, which validates the reliability of those obtained mode shape values. Using these results, the optimal effective vibration length of each mode for three different sensor deployments can be decided.

Considering the guidelines for mode selection as described in the previous section, the 2nd, 4th, and 5th modes are picked for the case of 1/2 coverage to estimate the corresponding tension and flexural rigidity. Similarly, the 3rd to 5th modes are used for the case of 1/3 coverage. But in the case of full coverage, the 2nd to 4th modes are adopted. The fitted results of the above selected modes for the full and 1/3 coverages are compared in Figure 9. With these choices, Table 10 shows that the estimated values of tension for Cable CR06 based on the 1/2 and 1/3 covering ranges of measurements are 4088 kN and 4096 kN, respectively. Taking the

TABLE 9: Estimated tension and accuracy for Cable SF100 of Kao-Ping-Hsi Bridge.

Covering range of measurements	Selected mode	Modal frequency (Hz)	Effective vibration length (m)	Estimated tension (kN)	Percentage of error (%)
1/4	4	1.229	317.883		
	5	1.537	317.714	4975.4	−0.16
	7	2.156	318.045		
	8	2.466	317.944		
	9	2.777	317.926	4986.0	0.05
	12	3.718	317.965		
1/7	7	2.156	318.050		
	8	2.466	318.046	5000.9	0.35
	9	2.777	317.970		
	13	4.034	318.108		
	14	4.352	318.095	4998.2	0.30
	15	4.671	318.064		
1/10	10	3.090	318.176		
	11	3.403	318.275	4992.5	0.18
	12	3.718	318.268		
	13	4.034	318.323		
	17	5.316	318.371	5004.3	0.42
	18	5.641	318.096		

(a)

(b)
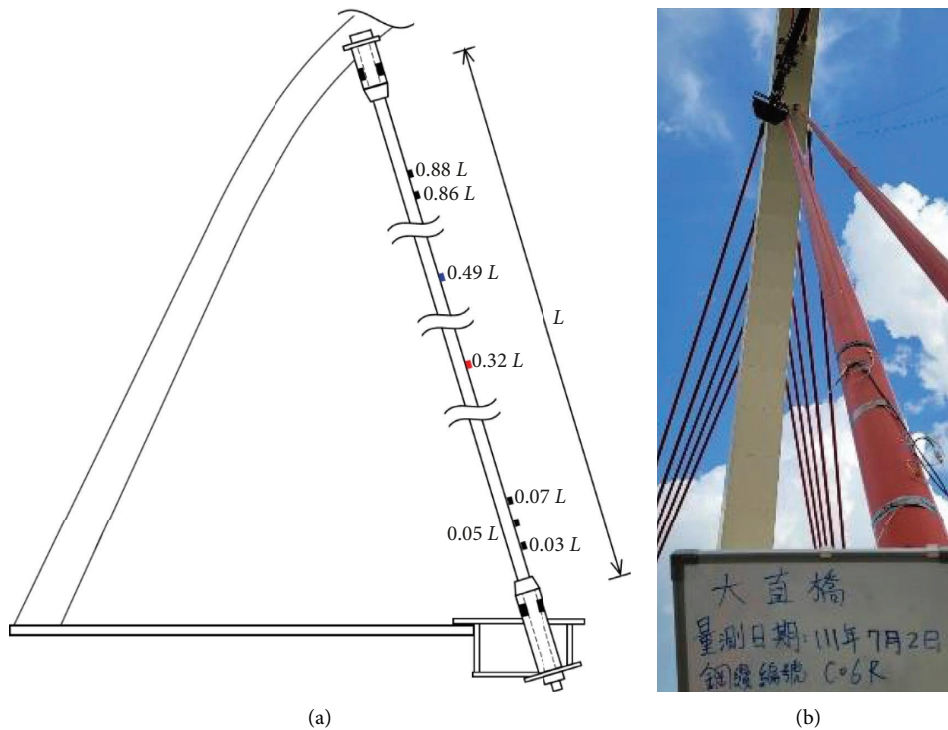
FIGURE 8: Sensor deployment for field measurements on Cable CR06 of Da-Chih Bridge. (a) Illustration. (b) Photo.

tension of 4081 kN obtained from the full coverage as the reference value, it is found that the errors for those determined from both partial coverages are 0.17% and 0.37%. Therefore, the field validation on Cable CR06 achieves an exceptional level of tension estimation accuracy for both partial coverages, which is not inferior to the results for the corresponding numerical investigations presented in Table 3 at all.

TABLE 10: Estimated tension for Cable CR06 of Da-Chih Bridge with real measurements.

Covering range of measurements	Selected mode	Frequency (Hz)	Effective vibration length (m)	Tension (kN) and error (%)
Full	2nd	5.140	41.534	4081
	3rd	7.777	41.356	
	4th	10.470	41.382	
1/2	2nd	5.140	41.423	4088 (0.17)
	4th	10.470	41.627	
	5th	13.244	41.211	
1/3	3rd	7.777	41.793	4096 (0.37)
	4th	10.470	40.809	
	5th	13.244	41.646	

(a)

(b)

(c)

(d)
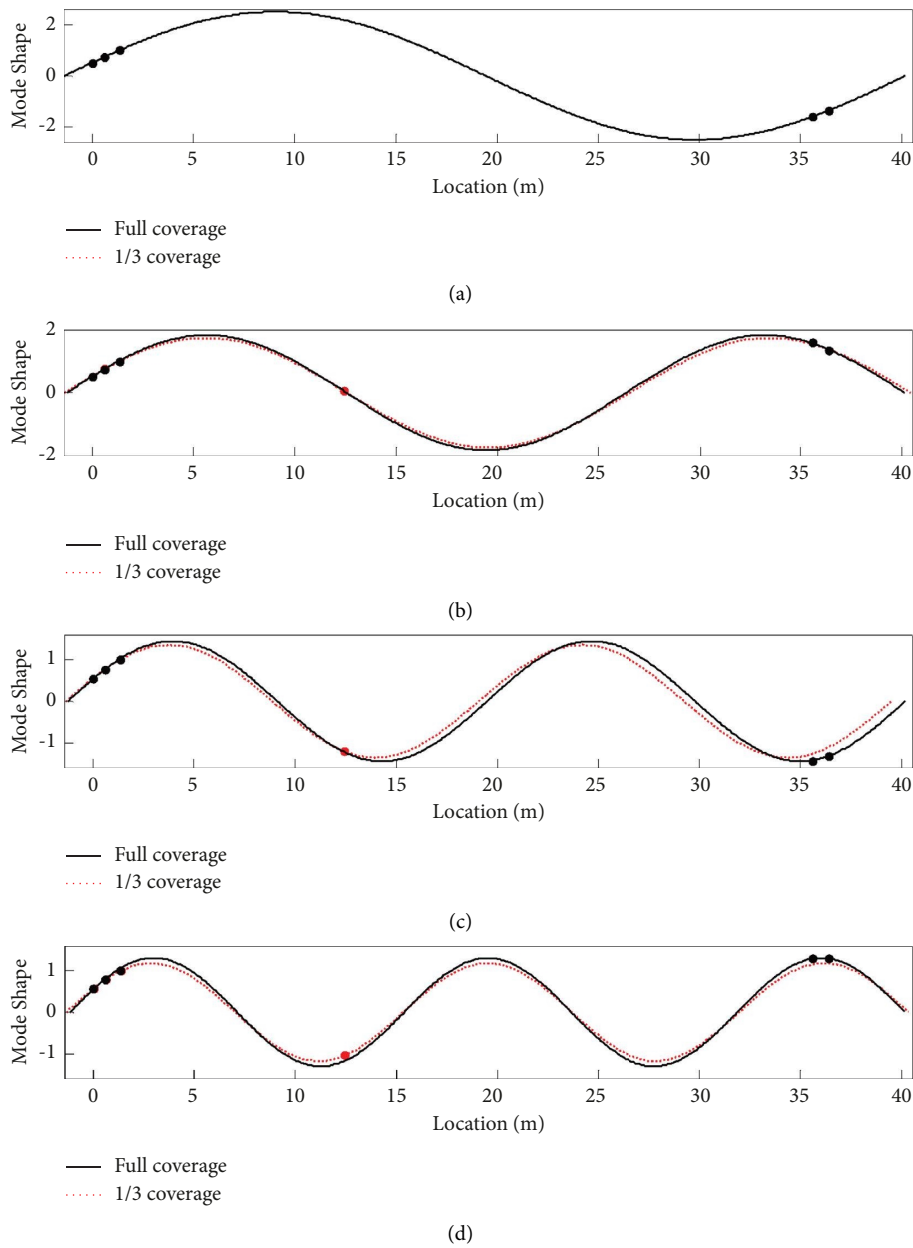
FIGURE 9: Optimally fitted sinusoidal functions of Cable CR06 with two sensor deployments. (a) Mode 2. (b) Mode 3. (c) Mode 4. (d) Mode 5.

4.2. Cable F07 of Shih-Chien Bridge. For Cable F07 of Shih-Chien Bridge, the high-resolution velocimeters (VSE-15D) made by Tokyo Sokushin were applied to measure its in-plane vibration signals also with a duration of 300 sec and a sampling rate of 200 Hz. The measurements with the full coverage and 1/4 coverage are considered in this case. These two sensor deployments are portrayed and photographed in Figure 10 where the three velocimeters close to the deck end were located at $x = 0.01L$, 0.03L, and 0.05L with the consideration of the higher value of $\varepsilon \approx 30000$ for Cable F07. The fourth velocimeter near the pylon end was installed at $x = 0.99L$ for the full coverage and at $x = 0.24L$ for the 1/4 coverage, respectively.

From the measurements taken on Cable F07, the modal frequencies and mode shape values of the first ten modes can be accurately identified except for the second mode. The 3rd to 5th modes are subsequently selected to obtain the corresponding tension and flexural rigidity in the case of full coverage, while the 4th, 5th, and 8th modes are employed for the case of 1/4 coverage. In addition to the fitted results of the above selected modes drawn in Figure 11 for both sensor deployments, Table 11 exhibits that the determined values of tension for Cable F07 with these two covering ranges of measurements are 751.6 kN and 758.3 kN, respectively. With a discrepancy of 0.89%, the field validation on Cable F07 also attains a fairly good accuracy for the 1/4 coverage in tension estimation which is comparable to that for the corresponding numerical investigations displayed in Table 5. It is clearly shown that the covering range of sensor deployment can be further reduced to 1/4 for this cable with a higher ε value of 30000 to maintain the error percentage below 1%. As for the 1/6 coverage that is also verified in the numerical results of Table 5 to reach the same standard, it is not performed in the real measurements on Cable F07 due to the limit of time. But since the error percentage of 0.89% for the 1/4 coverage has been very close to the threshold of 1%, it is not expected that the 1/6 coverage in practical applications would perform as well as its numerical counterpart.

4.3. Cables SB106 and SF100 of Kao-Ping-Hsi Bridge. Ambient vibration measurements were also conducted on Cables SB106 and SF100 of Kao-Ping-Hsi Bridge using the MEMS accelerometers (SDI2210-002) to record their in-plane vibration signals with a duration of 300 sec and a sampling rate of 200 Hz. As illustrated in Figure 12(a) together with an on-site photo in Figure 12(b), the measurements for Cable SB106 include three partial coverages (1/6, 1/4, and 1/3). The three accelerometers near the deck end were installed at $x = 0.01L$, 0.03L, and 0.05L considering the high value of $\varepsilon \approx 55000$ in this case. The fourth accelerometer at the far end was located at $x = 0.18L$ for 1/6 coverage and at $x = 0.26L$ for 1/4 coverage, respectively. Restricted by the 40 m height limit of the hired crane, it is

impossible to execute the full coverage for Cable SB106 with a total length of 160 m. But with the numerical simulation in Subsection 3.3 to achieve less than 0.2% of error in tension estimation and the field verification from Cable CR06 of Da-Chih Bridge in Subsection 4.1 to attain less than 0.4% of error, the estimated tension from the 1/3 coverage can be confidently taken to act for that from the full coverage as the reference value in evaluating the results obtained from the other partial coverages. Furthermore, two accelerometers were deployed at $x = 0.34L$ and 0.35L for the 1/3 coverage to reinforce the fitting accuracy at the far end.

The modal frequencies and mode shape values of the first twelve modes can be easily identified from the measurements on Cable SB106. As listed in Table 12, the effective vibration lengths for the 6th, 9th, and 10th modes are determined for the case of 1/3 coverage to solve its corresponding tension of 8384 kN. Besides, Table 12 also displays that the tension value of 8392 kN is decided from the 4th, 8th, and 9th modes for the case of 1/4 coverage, while the tension value of 8472 kN is obtained from the 6th, 9th, and 12th modes for the case of 1/6 coverage. Compared with the reference value from the 1/3 coverage, the errors for those gained from the 1/4 coverage and 1/6 coverage are 0.10% and 1.05%, respectively. It is no doubt that the accuracy in tension estimation remains superb for the 1/4 coverage in the case of Cable SB106. With an error of 1.05%, however, the field validation on this cable discloses that the 1/6 coverage may be the lower limit to keep a good accuracy level with the error under 1%. Even though the corresponding numerical results listed in Table 8 indicate that the 1/8 coverage may also cross the same hurdle for this cable, it is unlikely to occur in realistic applications with the interferences from several potential error sources.

For Cable SF100 with a total length of 327 m, its measurement is merely feasible to cover the 1/4 range of the cable at most under the height limit of the hired crane. Because the corresponding numerical analysis in the previous section and the field validation from Cable SB106 both reach an excellent level with less than 0.2% of error in tension estimation, the estimated tension from the 1/4 coverage can be utilized to serve as the reference value in this case. Accordingly, the sensor deployments of two partial coverages (1/7 and 1/4) were adopted for Cable SF100 as shown in Figure 13 where the three accelerometers close to the deck end were located at $x = 0.01L$, 0.03L, and 0.05L. The fourth accelerometer at the far end was installed at $x = 0.15L$ for the 1/7 coverage. Similar to the situations in the case of Cable SB106, two accelerometers were deployed at $x = 0.25L$ and 0.26L for the 1/4 coverage to enhance the fitting accuracy at the far end.

With the measurements on Cable SF100, the modal frequencies and mode shape values of the first twenty modes can be identified without difficulty. As arranged in Table 13,
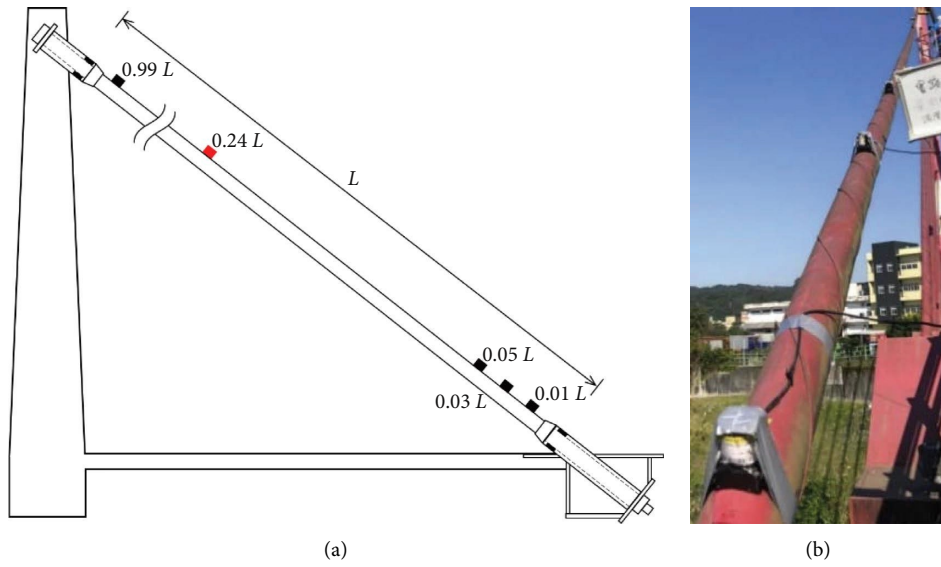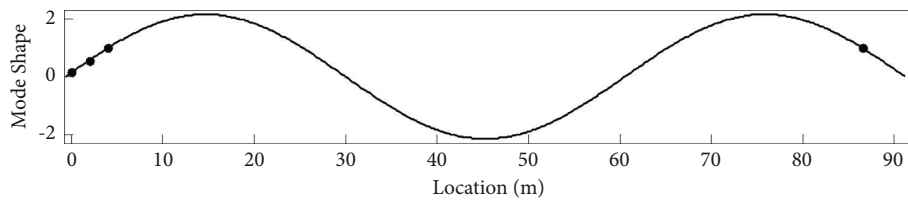
(a)   (b)

FIGURE 10: Sensor deployment for field measurements on Cable F07 of Shih-Chien Bridge. (a) Illustration. (b) Photo.
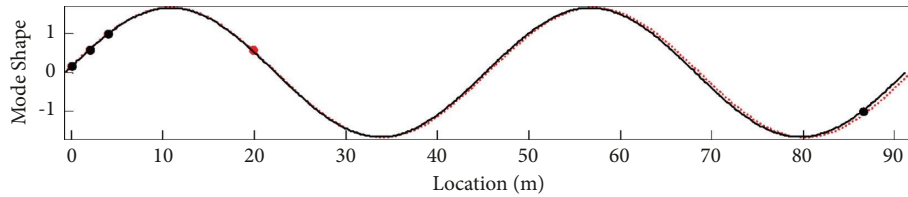
TABLE 11: Estimated tension for Cable F07 of Shih-Chien Bridge with real measurements.

Covering range of measurements	Selected mode	Frequency (Hz)	Effective vibration length (m)	Tension (kN) and error (%)
Full	3rd	2.260	91.748	
	4th	3.013	91.810	751.6
	5th	3.767	91.818	
1/4	4th	3.013	92.440	
	5th	3.767	92.413	758.3 (0.89)
	8th	6.093	92.089	

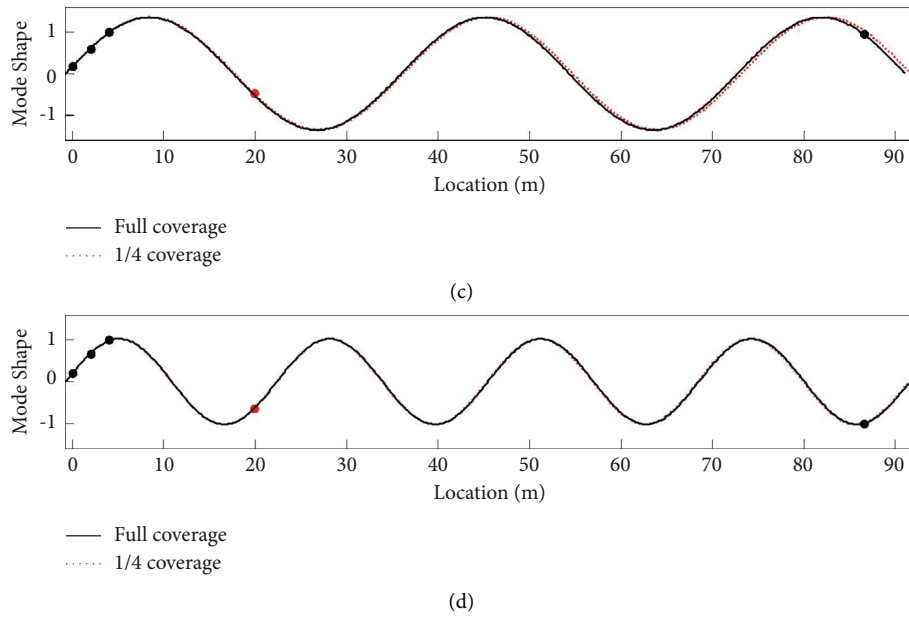(a)

(b)

FIGURE 11: Continued.

(c)

(d)

FIGURE 11: Optimally fitted sinusoidal functions of Cable F07 with two sensor deployments. (a) Mode 3. (b) Mode 4. (c) Mode 5. (d) Mode 8.
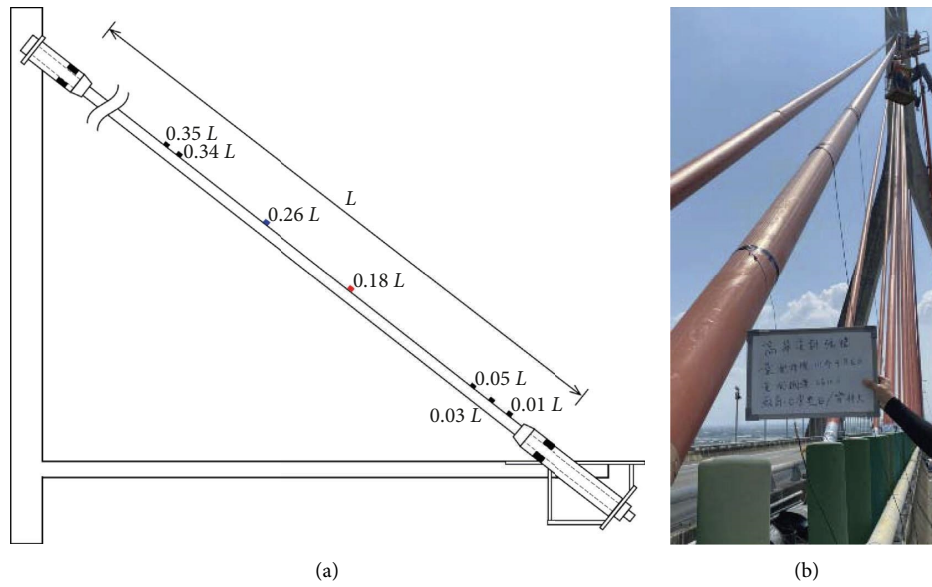

FIGURE 12: Sensor deployment for field measurements on Cable SB106 of Kao-Ping-Hsi Bridge. (a) Illustration. (b) Photo.

the 4th, 8th, and 9th modes are chosen for the case of 1/4 coverage to get their effective vibration lengths from fitting and then decide the corresponding tension of 4955 kN. It is also exhibited in Table 13 that the tension value of 5001 kN is obtained from the 7th, 15th, and 16th modes for the case of 1/7 coverage. Consequently, the field validation on Cable SF100 reveals 0.93% of error in tension estimation for the 1/7 coverage. Such results suggest that the 1/7 coverage seems to

TABLE 12: Estimated tension for Cable SB106 of Kao-Ping-Hsi Bridge with real measurements.

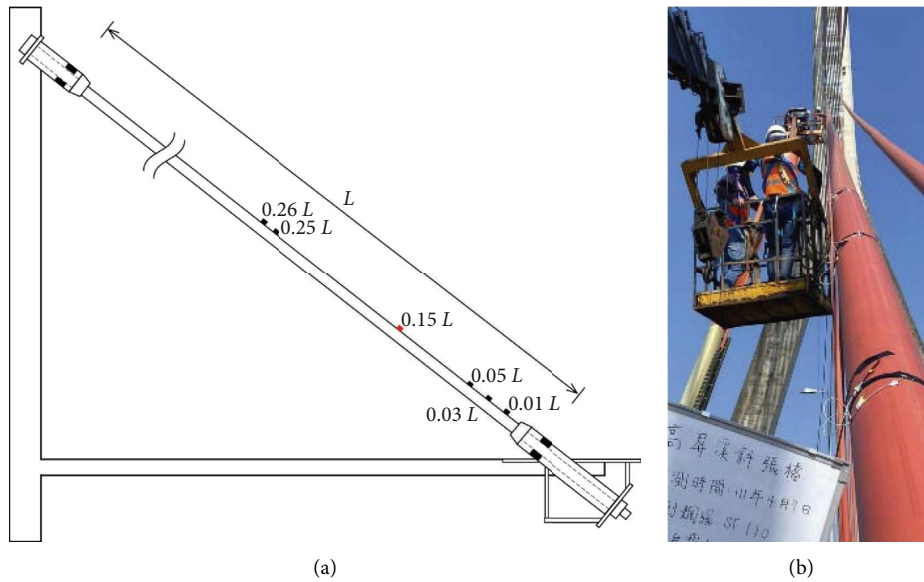| Covering range of measurements	Selected mode	Frequency (Hz)	Effective vibration length (m)	Tension (kN) and error (%)
1/3	6th	4.273	153.990	8384
	9th	7.110	153.949	
	10th	7.927	154.416	
1/4	4th	3.313	154.495	8392 (0.10)
	8th	6.320	153.757	
	9th	7.110	155.085	
1/6	6th	4.273	154.442	8472 (1.05)
	9th	7.110	154.418	
	12th	9.533	154.503	

FIGURE 13: Sensor deployment for field measurements on Cable SF100 of Kao-Ping-Hsi Bridge. (a) Illustration. (b) Photo.

TABLE 13: Estimated tension for Cable SF100 of Kao-Ping-Hsi Bridge.

Covering range of measurements	Selected mode	Frequency (Hz)	Effective vibration length (m)	Tension (kN) and error (%)
1/4	4th	1.227	317.603	4955
	8th	2.477	317.632	
	9th	2.777	318.090	
1/7	7th	2.163	316.897	5001 (0.93)
	15th	4.657	318.236	
	16th	4.977	317.389	

be the lower limit to hold the error under 1% for this extremely long cable with $\varepsilon \approx 80000$. Again, the performance in practical applications deteriorates a little bit compared with the corresponding numerical outcomes presented in Table 9.

5. Conclusions

To assess the applicability of the tension estimation method using local vibration measurements in a thorough manner, this research work is devoted to systematically investigate the appropriate covering ranges of measurements for different cables with a variety of slenderness. Four cables of three cable-stayed bridges are deliberately chosen to cover a wide range of the cable slenderness parameter ε. Numerical analyses with FE models and field validations with real measurements are conducted for these stay cables to demonstrate that the covering range of local measurements can be undoubtedly reduced with the increase of cable slenderness. In other words, longer cables would benefit more from this simplified method by more significantly dropping the sensor installation height. As for shorter cables

with inferior slenderness, the measurement with a full covering range usually does not cause any difficulty and it is typically not necessary to consider the method with local vibration measurements.

While the results in the current study do indicate that the efficacy of the method with local vibration measurements may be slightly diminished in practical applications compared with the corresponding numerical simulations, its excellent performance in field validations is still encouraging and provides crucial guidelines for determining the covering range of real measurements. For a relatively short cable with the slenderness parameter ε at the order of 4000, the adoption of 1/3 coverage is good enough to keep a high-level accuracy with at most 1% of error compared with the full coverage. In addition, 1/4, 1/6, and 1/7 coverages are found adequate to maintain the same level of accuracy for longer cables with the slenderness parameter at the orders of 30000, 55000, and 80000, respectively. These recommendations represent a landmark advance with important practical implications of the tension estimation method based on multiple vibration measurements. It needs to be also noted that only a reasonable guess for the order of the slenderness parameter (or the cable tension) is sufficient for the developed method and this is normally not difficult to accomplish in practice by initial information collection before measurements.

Ultimately, it should be pointed out that the method with local vibration measurements is not restricted to alleviate the expense and hard work of installing contact sensors near the high end for the tension estimation method based on effective vibration lengths. This simplified method requiring only a partial coverage of the cable would be also favorable to improve the resolution and consequently the accuracy in the applications of advanced noncontact sensors, especially the vision-based techniques. Moreover, such a concept of employing local vibration measurements to fit partial mode shapes is also a key to expediently handle more involved cases. In fact, this methodology is currently extending to analyze the suspender system with linkages and the corresponding results will be soon reported. It is also expected that a convenient tension estimation approach for the stay cable system with crossties will be explored in the near future.

Data Availability

The data used to support the findings of this study are available from the corresponding author upon request.

Conflicts of Interest

The authors declare that they have no conflicts of interest.

Acknowledgments

References

[1] C. Gentile, "Application of microwave remote sensing to dynamic testing of stay-cables," *Remote Sensing*, vol. 2, no. 1, pp. 36–51, 2009.

[2] C. C. Chen, W. H. Wu, H. Z. Tseng, C. H. Chen, and G. Lai, "Application of digital photogrammetry techniques in identifying the mode shape ratios of stay cables with multiple camcorders," *Measurement*, vol. 75, pp. 134–146, 2015.

[3] Y. Tian, C. Zhang, S. Jiang, J. Zhang, and W. Duan, "Non-contact cable force estimation with unmanned aerial vehicle and computer vision," *Computer-Aided Civil and Infrastructure Engineering*, vol. 36, no. 1, pp. 73–88, 2021.

[4] Z. Ma, J. Choi, and H. Sohn, "Noncontact cable tension force estimation using an integrated vision and inertial measurement system," *Measurement*, vol. 199, Article ID 111532, 2022.

[5] J. Weng, L. Chen, L. Sun, Y. Zou, Z. Liu, and H. Guo, "Fully automated and non-contact force identification of bridge cables using microwave remote sensing," *Measurement*, vol. 209, Article ID 112508, 2023.

[6] M. A. Ceballos and C. A. Prato, "Determination of the axial force on stay cables accounting for their bending stiffness and rotational end restraints by free vibration tests," *Journal of Sound and Vibration*, vol. 317, no. 1-2, pp. 127–141, 2008.

[7] Z. Fang and J. Q. Wang, "Practical formula for cable tension estimation by vibration method," *Journal of Bridge Engineering*, vol. 17, no. 1, pp. 161–164, 2012.

[8] H. Zui, T. Shinke, and Y. Namita, "Practical formulas for estimation of cable tension by vibration method," *Journal of Structural Engineering*, vol. 122, no. 6, pp. 651–656, 1996.

[9] A. B. Mehrabi and H. Tabatabai, "Unified finite difference formulation for free vibration of cables," *Journal of Structural Engineering*, vol. 124, no. 11, pp. 1313–1322, 1998.

[10] H. Nam and N. T. Nghia, "Estimation of cable tension using measured natural frequencies," *Procedia Engineering*, vol. 14, pp. 1510–1517, 2011.

[11] W. X. Ren, G. Chen, and W. H. Hu, "Empirical formulas to estimate cable tension by cable fundamental frequency," *Structural Engineering and Mechanics*, vol. 20, no. 3, pp. 363–380, 2005.

[12] A. A. Sagues, S. C. Kranc, and T. G. Eason, "Vibrational tension measurement of external tendons in segmental posttensioned bridges," *Journal of Bridge Engineering*, vol. 11, no. 5, pp. 582–589, 2006.

[13] Y. H. Huang, J. Y. Fu, R. H. Wang, Q. Gan, R. Rao, and A. R. Liu, "Practical formula to calculate tension of vertical cable with hinged-fixed conditions based on vibration method," *J Vibroeng*, vol. 16, no. 2, pp. 997–1009, 2014.

[14] Y. H. Huang, J. Y. Fu, R. H. Wang, Q. Gan, and A. R. Liu, "Unified practical formulas for vibration-based method of cable tension estimation," *Advances in Structural Engineering*, vol. 18, no. 3, pp. 405–422, 2015.

[15] R. Geier, G. De Roeck, and R. Flesch, "Accurate cable force determination using ambient vibration measurements," *Structure and Infrastructure Engineering*, vol. 2, no. 1, pp. 43–52, 2006.

[16] B. H. Kim and T. Park, "Estimation of cable tension force using the frequency-based system identification method," *Journal of Sound and Vibration*, vol. 304, no. 3-5, pp. 660–676, 2007.

[17] W. Liao, Y. Ni, and G. Zheng, "Tension force and structural parameter identification of bridge cables," *Advances in Structural Engineering*, vol. 15, no. 6, pp. 983–995, 2012.

[18] L. Ma, "A highly precise frequency-based method for estimating the tension of an inclined cable with unknown boundary conditions," *Journal of Sound and Vibration*, vol. 409, pp. 65–80, 2017.

[19] A. Pacitti, M. Peigney, F. Bourquin, and W. Lacarbonara, "Cable tension identification via nonlinear static inverse problem," *Structural Health Monitoring*, vol. 20, no. 2, pp. 546–566, 2021.

[20] L. X. Le, D. M. Siringoringo, H. Katsuchi, and Y. Fujino, "Stay cable tension estimation of cable-stayed bridge under limited information on cable properties using artificial neural networks," *Structural Control and Health Monitoring*, vol. 29, no. 10, Article ID e3015, 2022.

[21] S. Wangchuk, D. M. Siringoringo, and Y. Fujino, "Modal analysis and tension estimation of stay cables using non-contact vision-based motion magnification method," *Structural Control and Health Monitoring*, vol. 29, no. 7, Article ID e2957, 2022.

[22] D. Jana and S. Nagarajaiah, "Computer vision-based real-time cable tension estimation in Dubrovnik cable-stayed bridge using moving handheld video camera," *Structural Control and Health Monitoring*, vol. 28, no. 5, Article ID e2713, 2021.

[23] D. Jana, S. Nagarajaiah, and Y. Yang, "Computer vision-based real-time cable tension estimation algorithm using complexity pursuit from video and its application in Fred-Hartman cable-stayed bridge," *Structural Control and Health Monitoring*, vol. 29, no. 9, Article ID e2985, 2022.

[24] W. H. Wu, C. C. Chen, S. L. Lin, and G. Lai, "A real-time monitoring system for cable tension with vibration signals based on an automated algorithm to sieve out reliable modal frequencies," *Structural Control and Health Monitoring*, vol. 2023, Article ID 9343343, 25 pages, 2023.

[25] W. H. Wu, C. C. Chen, M. R. Leu, and G. Lai, "Determination of stay cable force based on multiple vibration measurements to consider the effects of uncertain boundary constraints," in *Proceedings of the 5th European Workshop on Structural Health Monitoring (5EWSHM)*, Sorrento, Italy, July 2010.

[26] C. C. Chen, W. H. Wu, C. H. Huang, and G. Lai, "Determination of stay cable force based on effective vibration length accurately estimated from multiple measurements," *Smart Structures and Systems*, vol. 11, no. 4, pp. 411–433, 2013.

[27] C. C. Chen, W. H. Wu, M. R. Leu, and G. Lai, "Tension determination of stay cable or external tendon with complicated constraints using multiple vibration measurements," *Measurement*, vol. 86, pp. 182–195, 2016.

[28] W. H. Wu, C. C. Chen, Y. C. Chen, G. Lai, and C. M. Huang, "Tension determination for suspenders of arch bridge based on multiple vibration measurements concentrated at one end," *Measurement*, vol. 123, pp. 254–269, 2018.

[29] C. C. Chen, W. H. Wu, S. Y. Chen, and G. Lai, "A novel tension estimation approach for elastic cables by elimination of complex boundary condition effects employing mode shape functions," *Engineering Structures*, vol. 166, pp. 152–166, 2018.

[30] C. C. Chen, W. H. Wu, Y. T. Liu, and G. Lai, "A convenient cable tension estimation method simply based on local vibration measurements to fit partial mode shapes," *Engineering Structures*, vol. 272, Article ID 115008, 2022.

[31] C. P. Yu, J. Lai, C. C. Cheng, and C. H. Chiang, "Direct evaluation of effective lengths of vibrating cables using responses from dual/three transducers," *Journal of Applied Science and Engineering, Section A*, vol. 16, no. 1, pp. 51–60, 2013.

[32] C. P. Yu, "Tension prediction for straight cables based on effective vibration length with a two-frequency approach," *Engineering Structures*, vol. 222, Article ID 111121, 2020.

[33] M. I. Syamsi, C. Y. Wang, and V. S. Nguyen, "Tension force identification for cable of various end-restraints using equivalent effective vibration lengths of mode pairs," *Measurement*, vol. 197, Article ID 111319, 2022.

[34] B. Yan, J. Yu, and M. Soliman, "Estimation of cable tension force independent of complex boundary conditions," *Journal of Engineering Mechanics*, vol. 141, no. 1, Article ID 6014015, 2015.

[35] B. Yan, W. Chen, J. Yu, and X. Jiang, "Mode shape-aided tension force estimation of cable with arbitrary boundary conditions," *Journal of Sound and Vibration*, vol. 440, pp. 315–331, 2019.

[36] B. Yan, D. Li, W. Chen, L. Deng, and X. Jiang, "Mode shape-aided cable force determination using digital image correlation," *Structural Health Monitoring*, vol. 20, no. 5, pp. 2430–2445, 2021.

[37] W. Chen, B. Yan, J. Liao, L. Luo, and Y. Dong, "Cable force determination using phase-based video motion magnification and digital image correlation," *International Journal of Structural Stability and Dynamics*, vol. 22, no. 7, Article ID 2250036, 2022.

[38] L. Chen, Y. Xu, and L. Sun, "A component mode synthesis method for reduced-order modeling of cable networks in cable-stayed bridges," *Journal of Sound and Vibration*, vol. 491, Article ID 115769, 2021.

[39] M. Geuzaine, F. Foti, and V. Denoel, "Minimal requirements for the vibration-based identification of the axial force, the bending stiffness and the flexural boundary conditions in cables," *Journal of Sound and Vibration*, vol. 511, Article ID 116326, 2021.